The non-local Lotka–Volterra system with a top hat kernel — Part 1

Needham, D. J.; Billingham, J.

DOI:
10.1098/rspa.2023.0381

Document Version
Publisher's PDF, also known as Version of record

Citation for published version (Harvard):
Needham, DJ & Billingham, J 2023, 'The non-local Lotka–Volterra system with a top hat kernel — Part 1: dynamics and steady states with small diffusivity', *Proceedings of the Royal Society A*, vol. 479, no. 2277, 20230381. https://doi.org/10.1098/rspa.2023.0381

PROCEEDINGS A

royalsocietypublishing.org/journal/rspa

Research

Cite this article: Needham DJ, Billingham J. 2023 The non-local Lotka–Volterra system with a top hat kernel—Part 1: dynamics and steady states with small diffusivity. *Proc. R. Soc. A* **479**: 20230381.
https://doi.org/10.1098/rspa.2023.0381

Received: 29 May 2023
Accepted: 23 August 2023

Subject Areas:
applied mathematics

Keywords:
non-local reaction–diffusion equations, pattern formation

Author for correspondence:
J. Billingham
e-mail: john.billingham@nottingham.ac.uk

Electronic supplementary material is available online at https://doi.org/10.6084/m9.figshare.c.6825659.

THE ROYAL SOCIETY PUBLISHING

The non-local Lotka–Volterra system with a top hat kernel—Part 1: dynamics and steady states with small diffusivity

D. J. Needham[1] and J. Billingham[2]

[1]School of Mathematics, University of Birmingham, Birmingham B15 2TT, UK
[2]School of Mathematical Sciences, University of Nottingham, Nottingham NG7 2RD, UK

JB, 0000-0002-4392-5770

We study the dynamics of the non-local Lotka–Volterra system $u_t = D_u u_{xx} + u(1 - \phi * u - \alpha v)$, $v_t = D_v v_{xx} + v(1 - \phi * v - \beta u)$, where a star denotes the spatial convolution and the kernel ϕ is a top hat function. We initially focus on the case of small, equal diffusivities ($D = D_u = D_v \ll 1$) together with weak interspecies interaction ($\alpha,\ \beta \ll 1$), and specifically $\alpha, \beta \ll D$. This can then be extended to consider small, but unequal, diffusivities and weak interactions, with now $\alpha, \beta \ll D_u, D_v \ll 1$. Finally, we are able to develop the theory for the situation when the diffusivities remain small, but the interactions become stronger. In each case, we find that u and v independently develop into periodic spatial patterns that consist of separated humps on an $O(1)$ time scale, and that these patterns become quasi-steady on a time scale proportional to the inverse diffusivity. These then interact on a longer time scale proportional to the inverse interaction scale, and approach a meta-stable state. Finally, a stable steady state is achieved on a much longer timescale, which is exponentially large relative to the preceding time scales. We are able to quantify this interaction process by determining a planar dynamical system that governs the temporal evolution of the separation between the two periodic arrays of humps on these sequentially algebraically and then exponentially long time scales. We find that, once the humps no longer overlap, the subsequent

dynamics lead to a symmetric disposition of the humps, occurring on the exponentially long time scale. Numerical solutions of the full evolution problem cannot access the behaviour on this final extreme time scale, but it can be fully explored through the dynamical system.

1. Introduction

In this paper, we study the simplest and most natural extension of the classical Lotka–Volterra population competition model to account for non-local effects, which are naturally present in the respective saturation terms. In particular, we study the case where intraspecies competition is non-local, while interspecies competition is local. A biological example might be two species of birds for which intraspecies competition for species-specific resources occurs over some spatial range, but interspecies competition occurs locally through competition for nesting sites.

The effect of the two non-local terms is to introduce two additional non-local length scales into the model, and we restrict attention to the simplest case when these two length scales are equal, so the two non-local ranges are close for both species. In population modelling terms, it should be expected that, in general, the kernel associated with the non-local effects is non-negative, symmetric and non-increasing with distance from its origin. With this in mind, we focus our attention here on the compactly supported top-hat kernel, as the simplest canonical representative of kernels that have these features. This simplicity allows us to develop both a qualitative and quantitative, asymptotic description of the dynamics of the solution, whose qualitative features (hump formation, hump sliding, metastability of edge touching hump states and subsequent separation on an exponentially long time scale to a final asymptotically stable state), which have previously been unidentified, are expected to remain relevant for other localized kernels that are less amenable to this type of analysis.

Previous studies of non-local systems of reaction–diffusion equations that model interacting populations have used many different functional forms for the interaction kernels and the local interaction terms (see [1–5] and references therein for some examples), and usually focus on linear stability analysis of steady states and numerical results on pattern formation. The results presented in [2], which are for a more general form of the equations studied below, are of particular relevance, since they note the existence of 'half-cosine' solutions, which are consistent with the results presented below and in [6]. The focus of the present paper is on the long time dynamics of the periodic solutions that develop on an $O(1)$ time scale and the later, exponentially slow dynamics that are not computationally accessible.

In dimensionless variables, with lengths made dimensionless on the non-local length scale, the coupled non-local reaction–diffusion system the we consider is

$$u_t = D_u u_{xx} + u(1 - J(u)(x,t) - \alpha v) \tag{1.1}$$

and

$$v_t = D_v v_{xx} + v(1 - J(v)(x,t) - \beta u), \tag{1.2}$$

for, with $T > 0$,

$$(x,t) \in D_T = \{(x,t) \in \mathbb{R}^2 : x \in \mathbb{R}, t \in (0,T]\}, \tag{1.3}$$

where, with the top-hat kernel,

$$\phi(y) = \begin{cases} 1, & |y| \le \frac{1}{2}, \\ 0, & |y| > \frac{1}{2}, \end{cases} \tag{1.4}$$

we have, for any $h \in C(\overline{D}_T)$,

$$J(h)(x,t) \equiv (\phi * h)(x,t) = \int_{x-(1/2)}^{x+(1/2)} h(y,t)\,\mathrm{d}y \quad \forall (x,t) \in \overline{D}_T. \tag{1.5}$$

The dimensionless diffusivities, D_u and D_v, measure the ratio of the diffusive length scales (based on the population growth time scale) to the non-local length scale, while the non-negative

parameters α and β measure the respective strengths of resource competition between the two species for u and v, respectively. The effects of the non-local structure compared with the effects of diffusion are most pronounced when D_u and D_v are small, so that the non-local length scale is much larger than the diffusive length scale, and it is this situation which the present paper principally addresses, in a regime far away from weakly nonlinear limits, and which addresses the fully nonlinear interaction between non-locality, diffusion and competition in the underlying non-local PDEs. Specifically, we consider the initial value problem formed from equations (1.1) and (1.2) with initial conditions,

$$u(x,0) = u_0(x) \tag{1.6}$$

and

$$v(x,0) = v_0(x), \tag{1.7}$$

for $x \in \mathbb{R}$, and boundary conditions,

$$u(x,t), v(x,t) \to 0 \text{ as } |x| \to \infty, \quad \text{uniformly for } t \in [0,T]. \tag{1.8}$$

Here, $u_0, v_0 : \mathbb{R} \to \mathbb{R}$ are non-trivial, non-negative, continuous and have compact support. Throughout, we consider classical solutions, with $u, v \in C(\overline{D}_T) \cap C^{1,2}(D_T)$, and we will refer to this Cauchy problem as (IVP).

We now define

$$D = \max\{D_u, D_v\}. \tag{1.9}$$

The principal focus of the paper will be the consideration of (IVP) when D is small, and formally $\alpha, \beta = o(D)$ as $D \to 0$, with particular attention to the large-t structure that emerges. To begin with, it is readily established, via the parabolic maximum principle on $\overline{D}_T$ (see, for example, [7]) that, for any solution to (IVP),

$$u(x,t), v(x,t) \geq 0 \quad \forall\, (x,t) \in \overline{D}_T, \tag{1.10}$$

while the parabolic comparison theorem then determines that,

$$u(x,t), v(x,t) \leq (\sup_{y\in\mathbb{R}}(u_0(y)) + \sup_{y\in\mathbb{R}}(v_0(y)))\, \mathrm{e}^t \quad \forall\, (x,t) \in \overline{D}_T. \tag{1.11}$$

The above *a priori* bounds on solutions to (IVP) consequently guarantee the uniqueness and existence of a global (on $\overline{D}_\infty$) solution to (IVP).

In relation to the study of (IVP), it is first important to recall the key salient features from the detailed study of the associated evolution problem for the scalar non-local Fisher–Kolmogorov equation, with top-hat kernel, referred to as (IBVP) in [6], and given by,

$$w_t = Dw_{xx} + w(1 - J(w)(x,t)), \quad (x,t) \in D_\infty, \tag{1.12}$$

$$w(x,0) = w_0(x), \quad x \in \mathbb{R} \tag{1.13}$$

and

$$w(x,t) \to 0 \text{ as } |x| \to \infty \quad \text{uniformly for } t \in [0,T], \text{ any } T > 0, \tag{1.14}$$

with $w_0 = u_0$ or v_0. In [6], it has been established that (IBVP) has a global solution $w : \overline{D}_\infty \to \mathbb{R}$, which is unique, and the nature of this solution has been examined in detail. In relation to the present paper, it is the structure of the large-t form of the solution to (IBVP), and in particular, *when the dimensionless diffusion coefficient D is small*, that is crucial. To summarize the results of [6], let $w : \overline{D}_\infty \to \mathbb{R}$ be the solution to (IBVP), then, for $t \geq O(D^{-1})$ there are three spatial regions in which the structure distinctly develops (see figures 3.1 and 3.2 of [6]), namely,

— Core region: $|x| = o(D^{1/2}t)$. In this region, a steady and stationary non-negative periodic state develops, with spatial wavelength $\lambda \approx 0.7$, and in particular

$$w(x,t) \sim F_p(x - x_0, \lambda, D), \tag{1.15}$$

with x_0 a constant (with $|x_0| \leq \frac{1}{2}\lambda$) depending upon the initial data. For even initial data, $x_0 = 0$ or $\frac{1}{2}\lambda$.

— Wavefront transition regions: $|x| = 2D^{1/2}t + O(1)$. In these symmetric regions, a wavefront propagates outwards into the unstable zero equilibrium state, with propagation speed $v(t) \sim 2D^{1/2}$. This wavefront has a temporally periodic structure, with period $T_p(t) \sim \lambda/2D^{1/2}$, and accommodates, via periodic shedding at the rear, the formation of the stationary periodic structure that is left behind.
— Far-field regions: $|x| \gg 2D^{1/2}t + O(1)$. In these symmetric regions, the final spatial decay to the zero equilibrium state takes place, and in particular,

$$w(x,t) \sim \frac{w_\infty^\pm}{(Dt)^{1/2}}\, \mathrm{e}^{-((x^2-4Dt^2)/4Dt)}, \tag{1.16}$$

with $w_\infty^\pm$ positive constants related to the initial data.

In the above, we have, from [6], for each wavelength $\lambda \in (1/2 + O(\sqrt{D}), 1 - O(D))$,

$$F_p(x,\lambda,D) \sim \begin{cases} \frac{\pi}{(2\lambda-1)} \cos\left(\frac{2\pi x}{2\lambda-1}\right), & 0 \le |x| < a(\lambda) \\ E(x,D), & a(\lambda) < |x| \le \frac{1}{2}\lambda, \end{cases} \tag{1.17}$$

as $D \to 0$ over one spatial wavelength λ, with $E(x,D)$, as given in [6], being exponentially small in D as $D \to 0$, and

$$a(\lambda) = \frac{1}{2}\left(\lambda - \frac{1}{2}\right). \tag{1.18}$$

It should also be noted, from [6], that the gradient and curvature discontinuities at $|x| = a(\lambda)$ are smoothed out across passive thin edge regions of spatial thickness $O(D^{1/4})$.

We now turn our attention back to (IVP). Specifically, we will consider the asymptotic structure of the solution to (IVP) in detail when,

$$\alpha = \psi(D)\overline{\alpha} \quad \text{and} \quad \beta = \psi(D)\overline{\beta}, \tag{1.19}$$

with $\psi(D) = o(D)$ as $D \to 0$, and $\overline{\alpha}, \overline{\beta} = O(1)$.

The paper is structured as follows. In §2, we consider the asymptotic solution of (IVP) when $D_u = D_v \equiv D \ll 1$, with $\alpha, \beta = o(D)$ as $D \to 0$. We show that a periodic solution develops, consisting of separated cosine humps in both u and v, which then interact over long time scales. We find that on these long time scales the leading order dynamics are controlled by an autonomous planar dynamical system, which indicates that once the humps have become non-overlapping, the dynamics of the subsequent separation are on an exponentially long time scale. The qualitatively similar asymptotic behaviour when $D_u \neq D_v$ is discussed in appendix A. In §3, we consider how this asymptotic theory is modified when $O(D) \le \alpha,\ \beta \le O(1)$. The theory developed in §§2 and 3 is compared with numerical solutions of (IVP) in §4, and found to be in good agreement. We conclude in §5.

2. Equal diffusivities: asymptotic solution to (IVP) as $D \to 0$ with $\psi(D) = o(D)$

In this section, we consider the asymptotic solution to (IVP) as $D \to 0$, with formally $\psi(D) = o(D)$, in the case when $D_u = D_v = D$. In fact, we will see later that the theory developed in this section remains accurate up to $\psi(D) = O(D)$ as $D \to 0$. Also results for $D_u \neq D_v$ are qualitatively similar, and we present a summary in appendix A. In this limit, the structure of the solution develops on a number of distinguished time scales, which we address in turn.

(a) $0 \le t \ll \psi(D)^{-1}$

We start in what we label as region I, where $0 \le t \ll \psi(D)^{-1}$ and $x \in \mathbb{R}$, as $D \to 0$. In this region, we write the solution to (IVP) as,

$$u(x,t;D) = u_I(x,t;D) + O(\psi(D)) \tag{2.1}$$

and

$$v(x,t;D) = v_I(x,t;D) + O(\psi(D)), \tag{2.2}$$

where we determine u_I and v_I so that these approximations remain uniform for $(x,t) \in \mathbb{R} \times [0, o(\psi(D)^{-1}))$ as $D \to 0$. On substituting into (IVP), the most structured balance is achieved when both of u_I and v_I satisfy, independently, the problem (IBVP), with $w_0 = u_0$ and $w_0 = v_0$, respectively. The detailed structure of each of u_I and v_I then follows from [6], and the summary provided in the introduction to the present paper. In particular, we observe, from (1.15) to (1.18), that there are constants x_u and x_v, depending upon u_0 and v_0, respectively, and independent of D, as $D \to 0$, for which,

$$u_I(x,t;D) \sim F_p(x - x_u, \lambda, D) \tag{2.3}$$

and

$$v_I(x,t;D) \sim F_p(x - x_v, \lambda, D), \tag{2.4}$$

with $t \ge O(D^{-1})$ and $|x| = o(D^{1/2}t)$, as $D \to 0$. Here, following [6], $\lambda \approx 0.7$, while $x_v \in [-\frac{1}{2}\lambda, \frac{1}{2}\lambda)$ and $(x_u - x_v) \in [-\frac{1}{2}\lambda, \frac{1}{2}\lambda)$. We observe, from (2.1) to (2.4), that both u and v develop, as $D \to 0$, into two identical spatially periodic steady states, with wavelength $\lambda \approx 0.7$, and each consisting of discrete symmetric cosine humps, with support length $2a(\lambda) = \lambda - \frac{1}{2}$, and each pair of humps separated by a dead region of length $\frac{1}{2}$, in which the periodic profile is exponentially small in D as $D \to 0$ (for further details, see [6]). This final periodic steady state develops on the time scale $t = O(D^{-1})$, with the *phase difference* between that representing u and that representing v being $(x_u - x_v)$. On considering the terms at $O(\psi(D))$ in expansions (2.1) and (2.2), we find that both terms have spatial L^∞ magnitude of $O(t)$ when t is large. We thus conclude that both of the expansions (2.1) and (2.2) become non-uniform when t is large, and in particular, on the scale

$$t = O(\psi(D)^{-1}). \tag{2.5}$$

On this long time scale, each of the respective periodic arrays of identical discrete humps remain fully coherent, with now just a slow change in the phase between the two periodic arrays taking place on and beyond the long time scale given in (2.5). It is this evolution in phase that we now consider.

(b) $t \ge O(\psi(D)^{-1})$

In this section, we introduce region *II*, in which now $t \ge O(\psi(D)^{-1})$ and $x \in \mathbb{R}$, as $D \to 0$. We anticipate that on this long time scale, the periodic arrays propagate in permanent form until the phase shift reaches an equilibrium state and a final steady state is reached. Thus we introduce the scaled time coordinate $\tau = \psi(D)t \ge O(1)$ and expand in region II in the form,

$$u(x,\tau;D) \sim F_p(x - s_u(\tau), \lambda, D) \tag{2.6}$$

and

$$v(x,\tau;D) \sim F_p(x - s_v(\tau), \lambda, D), \tag{2.7}$$

as $D \to 0$, with $x \in \mathbb{R}$ and $s_u, s_v : (0,\infty) \to \mathbb{R}$ to be determined, while, from above, $\lambda \approx 0.7$. We next rewrite equations (1.1) and (1.2) in terms of τ, and substitute from (2.6) and (2.7), recalling that

F_p is an exact steady state of each equation when $\bar{\alpha} = \bar{\beta} = 0$. Using the spatial periodicity, we can take,

$$s_v(0) = x_v \in \left[-\frac{1}{2}\lambda, \frac{1}{2}\lambda\right) \quad \text{with } (s_u(0) - s_v(0)) = (x_u - x_v) \in \left[-\frac{1}{2}\lambda, \frac{1}{2}\lambda\right), \tag{2.8}$$

and restrict attention to the dynamics of the first (relative to the spatial origin) cosine hump in v and its closest neighbouring cosine hump in u. We obtain, at leading order,

$$(F_p'(x - s_u, \lambda, D))^2 s_u' = \bar{\alpha} F_p'(x - s_u, \lambda, D) F_p(x - s_u, \lambda, D) F_p(x - s_v, \lambda, D) \tag{2.9}$$

and

$$(F_p'(x - s_v), \lambda, D)^2 s_v' = \bar{\beta} F_p'(x - s_v, \lambda, D) F_p(x - s_v, \lambda, D) F_p(x - s_u, \lambda, D), \tag{2.10}$$

for $x \in \mathbb{R}$ and $\tau > 0$. To obtain the evolution equations governing $s_u(\tau)$ and $s_v(\tau)$, we now integrate each of the above equations over one spatial wavelength, after which we obtain the two-dimensional, autonomous, dynamical system,

$$s_u' = \bar{\alpha} H(s_u - s_v, D) \tag{2.11}$$

and

$$s_v' = -\bar{\beta} H(s_u - s_v, D), \tag{2.12}$$

for $\tau > 0$, where $H \in C^1(\mathbb{R})$, is periodic with principal wavelength λ, and is given by,

$$H(Y, D) = \frac{1}{c} \int_{Y-(1/2)\lambda}^{Y+(1/2)\lambda} F_p'(w - Y, \lambda, D) F_p(w - Y, \lambda, D) F_p(w, \lambda, D)\, \mathrm{d}w, \tag{2.13}$$

for $Y \in \mathbb{R}$. Here, we note, using the evenness property of F_p, that H is an odd function, while the constant c is given by,

$$c = \int_{-(1/2)\lambda}^{(1/2)\lambda} (F_p'(l, \lambda, D))^2\, \mathrm{d}l. \tag{2.14}$$

In considering this dynamical system, it is convenient to introduce new dependent variables by the linear transformation,

$$\Delta = s_u - s_v \quad \text{and} \quad S = (\bar{\beta} s_u + \bar{\alpha} s_v)(\bar{\alpha} + \bar{\beta})^{-1}, \tag{2.15}$$

in terms of which the dynamical system becomes,

$$\Delta' = (\bar{\alpha} + \bar{\beta}) H(\Delta, D) \tag{2.16}$$

and

$$S' = 0, \tag{2.17}$$

for $\tau > 0$. We note that Δ measures the displacement on the x-axis between the centres of the neighbouring humps in, respectively, u and v, while S is the point on the x-axis which divides the line segment joining the peak locations of these respective neighbouring humps in the ratio $\bar{\alpha}$ to $\bar{\beta}$.

We can now construct the leading order asymptotic form of $H(\Delta, D)$ as $D \to 0$ for $\Delta \in [-\frac{1}{2}\lambda, \frac{1}{2}\lambda]$ via use of the detailed asymptotic structure of $F_p(Y, \lambda, D)$ as $D \to 0$, uniform over one wavelength $Y \in [-\frac{1}{2}\lambda, \frac{1}{2}\lambda]$, which was obtained in [6] (subsection 5.1). After considerable detailed, but straightforward, calculation, we obtain, as $D \to 0$,

$$H(\Delta, D) \sim \begin{cases} \frac{1}{3\pi}\left(1 + \cos\left(\frac{2\pi\Delta}{2\lambda-1}\right)\right)\sin\left(\frac{2\pi\Delta}{2\lambda-1}\right) & \text{for } \Delta \in A(D), \\ \operatorname{sgn}(\Delta)\Psi_\infty \frac{\gamma(|\Delta|)^2}{(2\lambda-1)^{3/2}\pi} D\, E(|\Delta|, D) & \text{for } |\Delta| \in B(D), \\ 2\operatorname{sgn}(\Delta)\Psi_\infty \frac{\gamma((1/2)\lambda)^2}{(2\lambda-1)^{3/2}\pi} D\, E(\frac{1}{2}\lambda, D) & \\ \quad \sinh\left(\frac{\gamma((1/2)\lambda)(|\Delta|-(1/2)\lambda)}{D^{1/2}}\right) & \text{for } |\Delta| \in C(D), \end{cases} \tag{2.18}$$

with,

$$E(\Delta, D) = \exp\left[-\frac{1}{D^{1/2}}\left\{\Phi\left(\frac{1}{4}\right) - \Phi\left(\lambda - \frac{1}{4} - \Delta\right)\right\}\right] \tag{2.19}$$

and

$$A(D) = \left(-\left(\lambda - \frac{1}{2}\right)\{1 - O(D^{1/4})\}, \left(\lambda - \frac{1}{2}\right)\{1 - O(D^{1/4})\}\right), \tag{2.20}$$

$$B(D) = \left(\left(\lambda - \frac{1}{2}\right)\{1 + O(D^{1/4})\}, \frac{1}{2}\lambda\{1 - O(D^{1/2})\}\right) \tag{2.21}$$

and

$$C(D) = \left(\frac{1}{2}\lambda\{1 - O(D^{1/2})\}, \frac{1}{2}\lambda\right]. \tag{2.22}$$

In (2.19), $\Phi : [0, \frac{1}{4}] \to \mathbb{R}$ is given by, for $\lambda \in [\frac{5}{8}, 1)$,

$$\Phi(s) = \frac{(2\lambda - 1)}{\pi}\left\{\cos\left(\frac{\pi(1-4s)}{4(2\lambda-1)}\right) - \cos\left(\frac{\pi}{4(2\lambda-1)}\right)\right\} \quad \forall\, s \in \left[0, \frac{1}{4}\right], \tag{2.23}$$

while, for $\lambda \in (\frac{1}{2}, \frac{5}{8})$,

$$\Phi(s) = \begin{cases} \frac{2\lambda-1}{\pi}\left\{\cos\left(\frac{\pi(1-4s)}{4(2\lambda-1)}\right) + 1\right\}, & s \in \left(\frac{5}{4} - 2\lambda, \frac{1}{4}\right], \\ 0, & s \in \left[0, \frac{5}{4} - 2\lambda\right]. \end{cases} \tag{2.24}$$

In addition,

$$\gamma(\Delta) = \Phi'\left(\lambda - \frac{1}{4} - \Delta\right) \quad \forall\, |\Delta| \in B(D). \tag{2.25}$$

We remark that $\Phi(s)$ is non-decreasing with $s \in [0, \frac{1}{4}]$, and $\Phi(0) = 0$. Significantly, we see that, as $D \to 0$, H is $O(1)$ when $\Delta \in A(D)$, but undergoes a rapid transition about $\Delta = \pm(\lambda - \frac{1}{2})$, to become exponentially small when $|\Delta| \in B(D) \cup C(D)$. It is important to note here that in this transition region , when $\Delta = (\lambda - \frac{1}{2})(1 \pm O(D^{1/4}))$, a calculation using the form for F_p in the edge layer, as detailed in [6], determines that $H(\Delta, D) = O(D^{3/4})$, and is *strictly positive*. Specifically, writing

$$\Delta = \left(\lambda - \frac{1}{2}\right) + (2\lambda - 1)^{1/2} D^{1/4} \overline{\Delta}, \tag{2.26}$$

with $\overline{\Delta} = O(1)$, and using the detailed structure of F_p in the edge region (see [6], §5.1) to compute (2.13), we obtain, after some lengthy but straightforward calculation, that

$$H(\overline{\Delta}, D) \sim \frac{D^{3/4}}{\pi^4(2\lambda - 1)^{3/2}} I(\overline{\Delta}), \tag{2.27}$$

as $D \to 0$ with $\overline{\Delta} = O(1)$. Here, the parameter free function $I : \mathbb{R} \to \mathbb{R}$ is given by,

$$I(X) = \int_{-\infty}^{\infty} |\Psi'(p)|\Psi(p)\Psi(X - p)\, \mathrm{d}p \quad \forall\, X \in \mathbb{R}, \tag{2.28}$$

with $\Psi : \mathbb{R} \to \mathbb{R}$ being the parameter free function defined in [6] (§5.1).

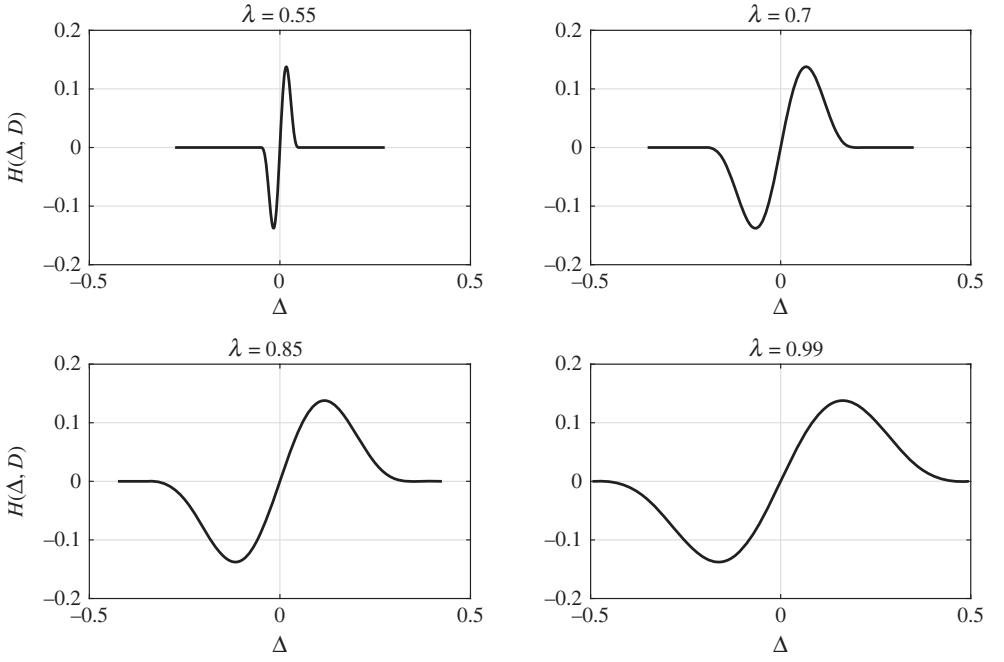

Figure 1. The function $H(\Delta, D)$ that appears on the right-hand side of (2.16), plotted for various values of λ and $D = 10^{-3}$. We took $\Psi_\infty = 1$, since, as discussed in [6], this $O(1)$ quantity is hard to determine numerically, and does not affect the form of the function outside the regions where it is exponentially small.

Returning to (2.16) and (2.17), we observe that a decoupling has taken place. Equation (2.17), with initial conditions (2.8), immediately gives,

$$S(\tau) = S_0 \equiv (\bar{\beta} x_u + \bar{\alpha} x_v)(\bar{\alpha} + \bar{\beta})^{-1} \quad \forall\, \tau > 0, \tag{2.29}$$

while (2.16) remains as a scalar autonomous dynamical system governing the temporal dynamics of $\Delta(\tau)$, subject to the initial condition,

$$\Delta(0) = \Delta_0 \equiv (x_u - x_v) \in \left[-\frac{1}{2}\lambda, \frac{1}{2}\lambda\right]. \tag{2.30}$$

The phase line diagram for this scalar dynamical system is shown in figure 1, using (2.18). equation (2.29) determines that the point on the x-axis that divides the line segment joining the respective peak locations of the humps in u and v in the ratio $\bar{\alpha}$ to $\bar{\beta}$ remains stationary at its initial location inherited from region I.

We now consider the dynamical system for $\Delta(\tau)$. It follows from (2.18), the initial condition (2.30) and figure 1 that we need only consider $\Delta \in [-\frac{1}{2}\lambda, \frac{1}{2}\lambda]$. On this interval, the scalar dynamical system has exactly three equilibrium points, at $\Delta = 0$ and $\Delta = \Delta_\pm \equiv \pm\frac{1}{2}\lambda$, each of which is hyperbolic. The equilibrium point at the origin is temporally unstable, while those at $\pm\frac{1}{2}\lambda$ are both asymptotically stable. However, since H is exponentially small in D at each point with $|\Delta| \in ((\lambda - \frac{1}{2}) + O((2\lambda - 1)^{1/2} D^{1/4}), \frac{1}{2}\lambda)$, the time scale in τ for motion along this part of the phase line is exponentially long in D as $D \to 0$, and so each such point can be regarded as a *metastable* pseudo-equilibrium point on the time scale $\tau = O(1)$ (figure 2). By contrast, those points on the phase line with $\Delta \in (-(\lambda - \frac{1}{2}) + O((2\lambda - 1)^{1/2} D^{1/4}), (\lambda - \frac{1}{2}) - O((2\lambda - 1)^{1/2} D^{1/4}))$ have $H = O(1)$, and so motion along this part of the phase line takes place, relatively, much more rapidly, on the scale $\tau = O(1)$. It is significant to note that the transition between this, relatively, *fast* and *exponentially slow* evolution in $\Delta(\tau)$, occurs at $\Delta \sim \pm(\lambda - \frac{1}{2})$, as $D \to 0$, which corresponds to the configuration when neighbouring humps in u and v, respectively, are support edge touching. The

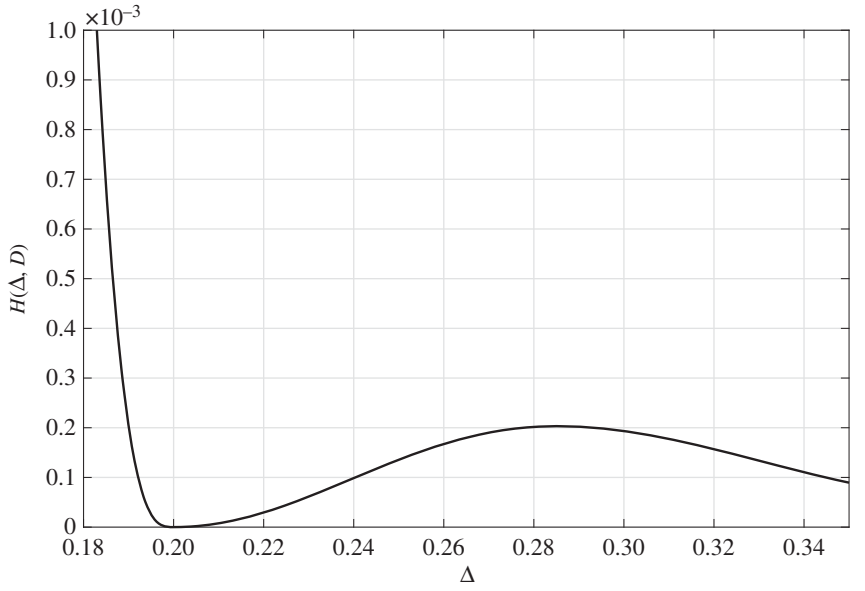

Figure 2. The function $H(\Delta, D)$ that appears on the right-hand side of (2.16), plotted for $\lambda = 0.7$ and $D = 10^{-3}$. This illustrates the behaviour of H for $\Delta \in B(D)$, where it is exponentially small.

fast dynamics occurs when these humps are overlapping, while the exponentially slow dynamics occur when their respective support intervals become separated.

We are now able to describe the evolution of $\Delta(\tau)$ from the initial condition (2.30). This depends wholly on $\Delta_0 \equiv (x_u - x_v)$, which is inherited from the evolution in region I, and *depends only on the initial data* u_0 and v_0, as $D \to 0$, with, in all circumstances, $\Delta_0 \in [-\frac{1}{2}\lambda, \frac{1}{2}\lambda]$. We have

— When $\Delta_0 = 0$, $\Delta(\tau) = 0$ for all $\tau \geq 0$.
— When $\Delta_0 \in (0, (\lambda - \frac{1}{2}))$, $\Delta(\tau)$ increases at an $O(1)$ rate with increasing $\tau = O(1)^+$, *until* $\tau = O(D^{-(1/2)})$, when $\Delta(\tau) = (\lambda - \frac{1}{2}) \pm O((2\lambda - 1)^{1/2} D^{1/4})$. On this algebraically large time scale in τ, of $O(D^{-(1/2)})$, $\Delta(\tau)$ continues to increase but now at the *algebraically slow* rate of $O(D^{3/4})$, with increasing τ, until $\tau \gg D^{-(1/2)}$, and $\Delta(\tau)$ has moved away from the edge touching displacement $\lambda - \frac{1}{2}$, and the two respective humps in u and v become separated, but not fully separated. The separation process now moves into its very slow final stage, with $\Delta(\tau)$ still increasing with τ, but now at an *exponentially slow* rate, as $D \to 0$. Ultimately, $\Delta(\tau)$ approaches its final equilibrium value of $\frac{1}{2}\lambda$, corresponding to the humps in u and v being fully separated and equally spaced from each other.
— When $\Delta_0 \in [\lambda - \frac{1}{2}, \frac{1}{2}\lambda)$, $\Delta(\tau)$ increases very slowly, on an *exponentially long* time scale in τ, and at an *exponentially slow* rate with τ, as $D \to 0$. Ultimately, $\Delta(\tau)$ approaches its final equilibrium value of $\frac{1}{2}\lambda$, corresponding to the humps in u and v being fully separated and equally spaced from each other.
— When $\Delta_0 = \frac{1}{2}\lambda$, $\Delta(\tau) = \frac{1}{2}\lambda$ for all $\tau \geq 0$.
— When $\Delta_0 \in [-\frac{1}{2}\lambda, 0)$, the behaviour of $\Delta(\tau)$ is precisely antisymmetric to the cases outlined above.

This completes the asymptotic solution to (IVP) as $D \to 0$. In appendix A, we show that it is straightforward to extend this analysis to the case where the diffusivities of the two species are small but not equal, with qualitatively similar results.

3. Extensions when α and β are of O(1) as $D \to 0$

We here consider (IVP) when the diffusion rates D_u and D_v are small, and possibly unequal (with D again defined as in (1.9)), but now both α and β are of $O(1)$, and so $\psi(D) = O(1)$ as $D \to 0$. As we will see in §4, numerical solutions suggest that spatially periodic hump formation also occurs in this case with, on a time scale of $t = O(D^{-1})$,

$$u(x, t; D) \sim F_p(x - x_u, \lambda, D) \tag{3.1}$$

and

$$v(x, t; D) \sim F_p(x - x_v, \lambda, D), \tag{3.2}$$

as $D \to 0$ with $x \in \mathbb{R}$, with $x_u \in [-\frac{1}{2}\lambda, \frac{1}{2}\lambda)$ and x_v within a wavelength of x_u. The process of hump formation and their dynamics is more complex in this case, and happens when $t = O(D^{-1})$ so that the respective periodic profiles move to a position with humps *touching*, when $\Delta_0 \equiv x_u - x_v = \pm(\lambda - \frac{1}{2})$ or *fully separated*, when $|\Delta_0| \in ((\lambda - \frac{1}{2}), \frac{1}{2}\lambda]$. Since the respective humps are now fully formed and, crucially, not overlapping, the dynamics on the time scale $t \gg D^{-1}$, is again on an exponentially long time scale as $D \to 0$, with,

$$u(x, t; D) \sim F_p(x - s_u(t), \lambda, D) \tag{3.3}$$

and

$$v(x, t; D) \sim F_p(x - s_v(t), \lambda, D), \tag{3.4}$$

as $D \to 0$, with $x \in \mathbb{R}$ and $s_u, s_v : (O(D^{-1}), \infty) \to \mathbb{R}$ to be determined by the dynamical system,

$$\Delta_t = \alpha H(\Delta, D_v) + \beta H(\Delta, D_u) \tag{3.5}$$

and

$$S_t = \frac{\alpha\beta}{(\alpha + \beta)}(H(\Delta, D_v) - H(\Delta, D_u)), \tag{3.6}$$

with $t > O(D^{-1})$. Here $|\Delta| \in C(D)$ and S remain as defined earlier, and H is as given in (2.18), being exponentially small in D as $D \to 0$. Thus, in all cases the solution evolves at an exponentially slow rate as $D \to 0$, as before, with $\Delta(t)$ approaching the final respective equilibrium position of $\pm\frac{1}{2}\lambda$ monotonically at this exponentially slow rate.

4. Numerical solutions of (IVP)

We now consider numerical solutions of (IVP) when D is small. These have been computed using MATLAB to implement a finite difference method with a uniform spatial grid. We truncate the infinite domain of solution and solve instead for $0 \le x \le L$, choosing to apply periodic boundary conditions at $x = 0$ and $x = L$. In §4(a), this allows us to focus on a single wavelength of the interaction of the spatially periodic solutions that we studied in §2. In subsequent subsections, the domain of solution is much longer, and we ensure that the spatial extent of the region where the solution is not small does not include either $x = 0$ or $x = L$, so that the boundary conditions do not affect the solution, with one exception, which we note below.

The non-local integral is evaluated using the trapezium rule. Time stepping is by either the explicit midpoint method or, if the timestep chosen is too large for numerical stability, a semi-implicit method, with the diffusion terms discretised using the Crank–Nicolson method. This guarantees second order accuracy in time. In order to accommodate both the rapid initial development of the solution (hump formation) and the subsequent slower development (hump sliding), we use adaptive timestepping. We adjust the timestep so that the maximum change in either u or v over one timestep is no larger than 10^{-2}. As with most one-dimensional reaction–diffusion problems, there is no great technical challenge involved in computing these numerical solutions.

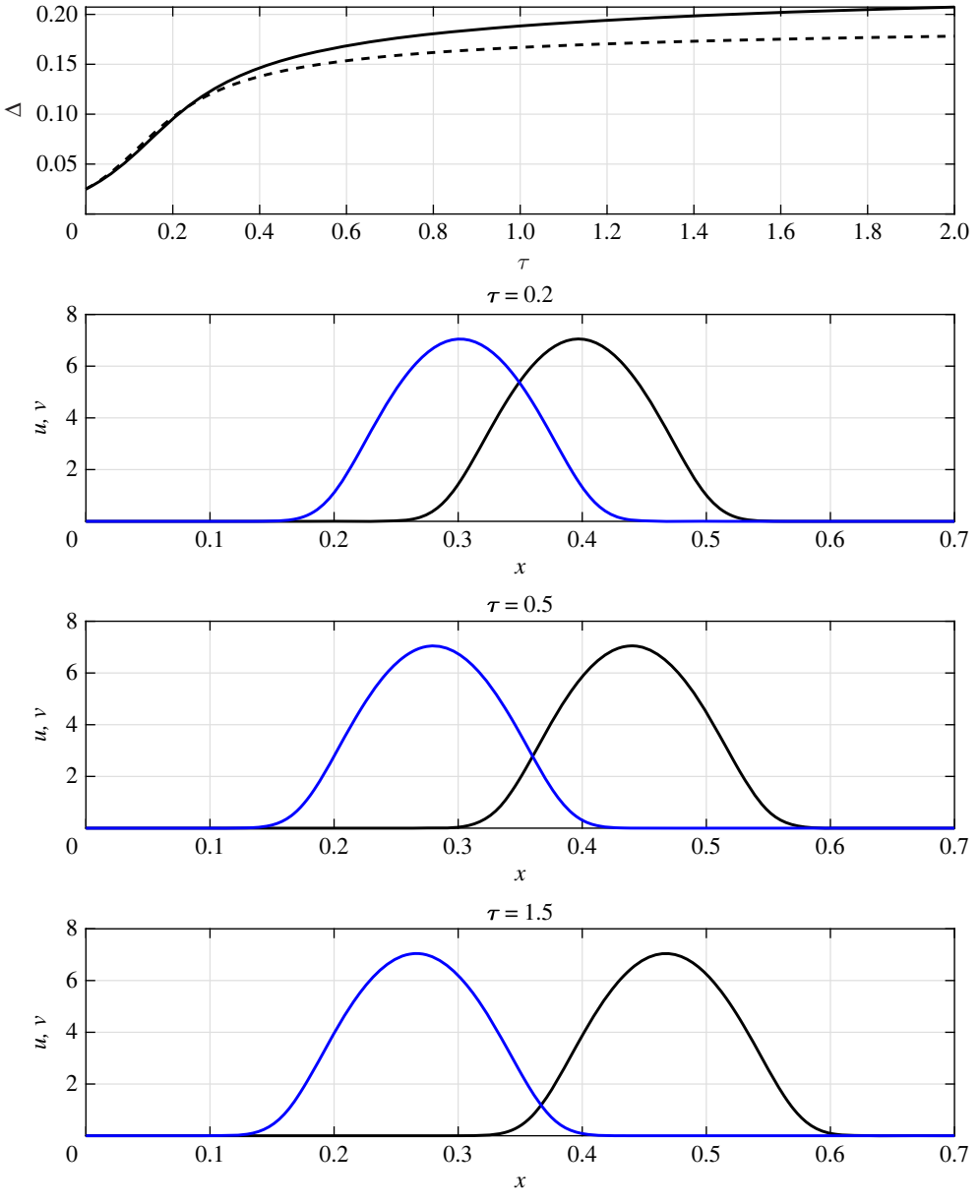

Figure 3. A comparison between the behaviour of the hump separation, Δ, as a function of $\tau = Dt$, determined from numerical solution of (2.16), shown by a broken line in the upper panel and from the full numerical solution of (IVP) on a domain of length 0.7 with periodic boundary conditions (solid line). The remaining three panels show the positions of the humps at various times (u as a blue line, v a black line), calculated from the full IVP, in each case with $D = 10^{-5}$, $\alpha = 2 \times 10^{-5}$ and $\beta = 10^{-5}$ and illustrate the slow separation of the humps on an $O(D^{-1})$ time scale.

(a) Dynamics with $\alpha, \beta \ll 1$

Figures 3 and 4 show the numerical solution of (IVP) on a periodic domain of length $L = 0.7$, the typical wavelength of solutions generated from localized initial conditions on an infinite domain. In these calculations, we have used the time variable $\tau = Dt$, so in relation to the theory of §2, this is equivalent to setting $\psi(D) = D$, and the formal validity of the theory then requires both $\overline{\alpha}$ and $\overline{\beta}$ to be taken as small.

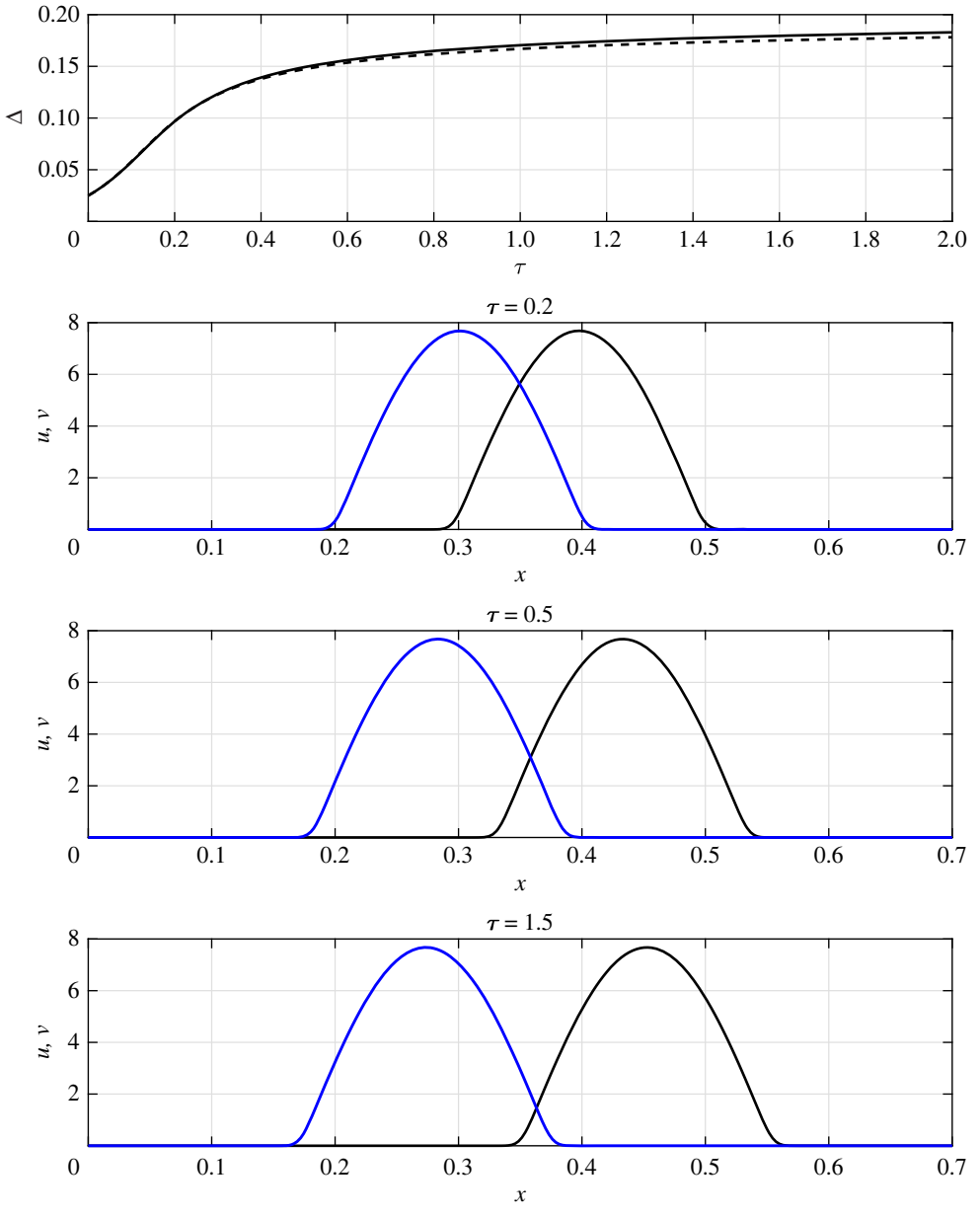

Figure 4. A comparison between the behaviour of the hump separation, Δ, as a function of $\tau = Dt$, determined from numerical solution of (2.16), shown by a broken line in the upper panel and from the full numerical solution of (IVP) on a domain of length 0.7 with periodic boundary conditions (solid line). The remaining three panels show the positions of the humps at various times (u as a blue line, v a black line), calculated from the full IVP, in each case with $D = 10^{-7}$, $\alpha = 2 \times 10^{-7}$ and $\beta = 10^{-7}$.

The initial conditions were taken as $u(x, 0) = F_p(x, \lambda, D)$, $v(x, 0) = F_p(x + s_0, \lambda, D)$, where F_p is the stable, steady periodic solution of the non-local Fisher–KPP equation (determined numerically) and s_0 is the initial hump separation. The development of a steady periodic solution from more general initial conditions is, because of the weak coupling, at leading order, the same as for two independent non-local Fisher–KPP equations, as described in [6]. By first studying these initial conditions, we are able to focus on the dynamics of the sliding humps and confirm the results of §2.

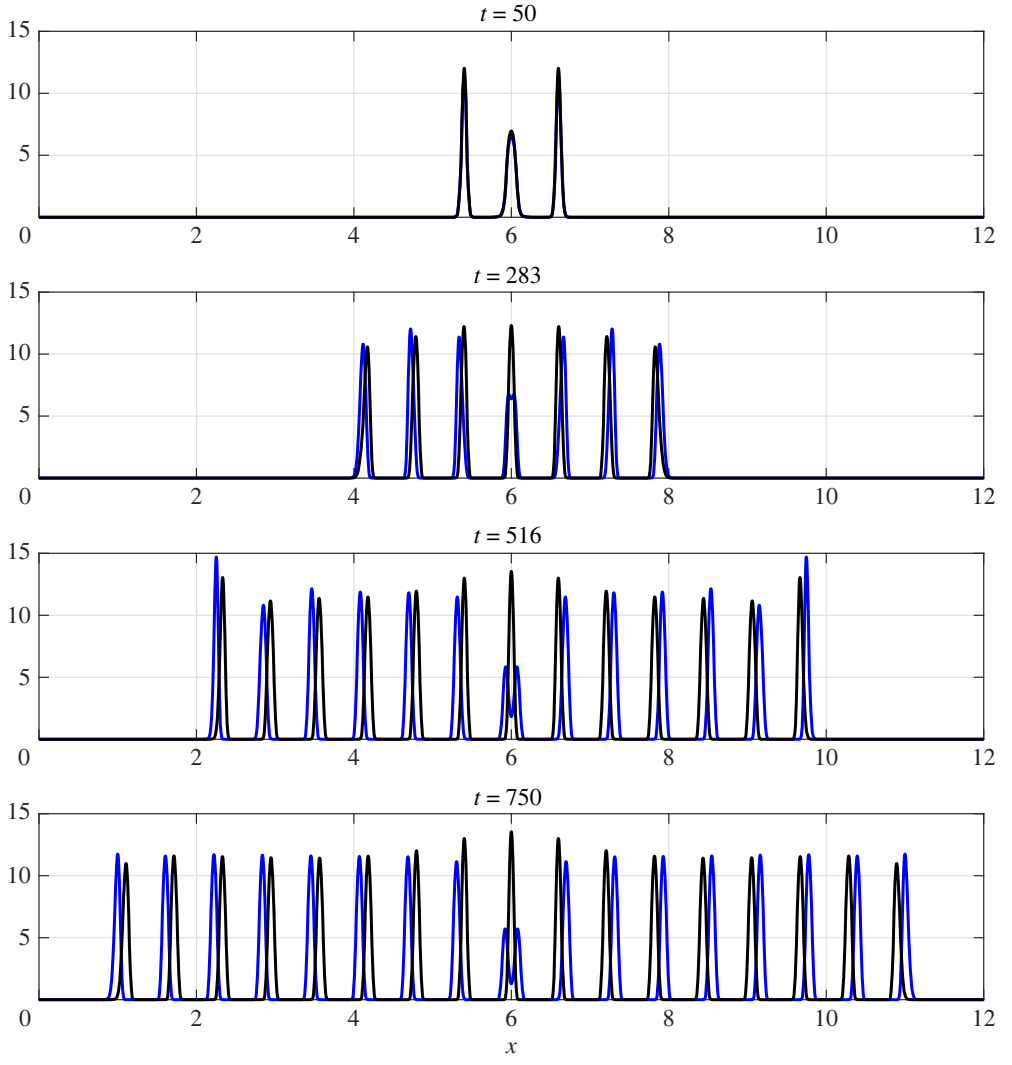

Figure 5. The numerical solution of (IVP) with $D_u = D_v = 10^{-5}$, $\alpha = 0.002$, $\beta = 0.001$ and equal initial data. The solution is shown when $t = 50, 283, 516$ and 750, with u drawn as a blue line and v a black line.

Numerical solutions are shown for an initial separation $s_0 = 0.025$, $\bar{\alpha} = 2$ and $\bar{\beta} = 1$ in figures 3 (with $D = 10^{-5}$) and 4 (with $D = 10^{-7}$). Although the theory presented in §2 is only strictly valid for α, $\beta = o(D)$, and hence (since, for convenience, here we have taken $\psi(D) = D$) $\bar{\alpha}$, $\bar{\beta}$ small, we find that we can verify the theoretical results even for the $O(1)$ values used in figures 3 and 4 (and naturally for smaller values as well). These demonstrate that the humps do indeed slide across each other on and beyond an $O(D^{-1})$ time scale until the region of overlap becomes sufficiently small, when there is a drastic slowing down of the rate of separation. Moreover, the upper panels of the figures, in which the separation, Δ, of the humps is plotted as a function of $\tau = Dt$, show that the quantitative form of the separation dynamics is in excellent agreement with the asymptotic theory presented in §2. The separation shown as a broken line in the upper panels is calculated by solving the autonomous, first order ordinary differential equation (2.16) numerically using *ode45* in MATLAB. As expected, the agreement between the asymptotic theory and the full numerical solution improves as D becomes smaller.

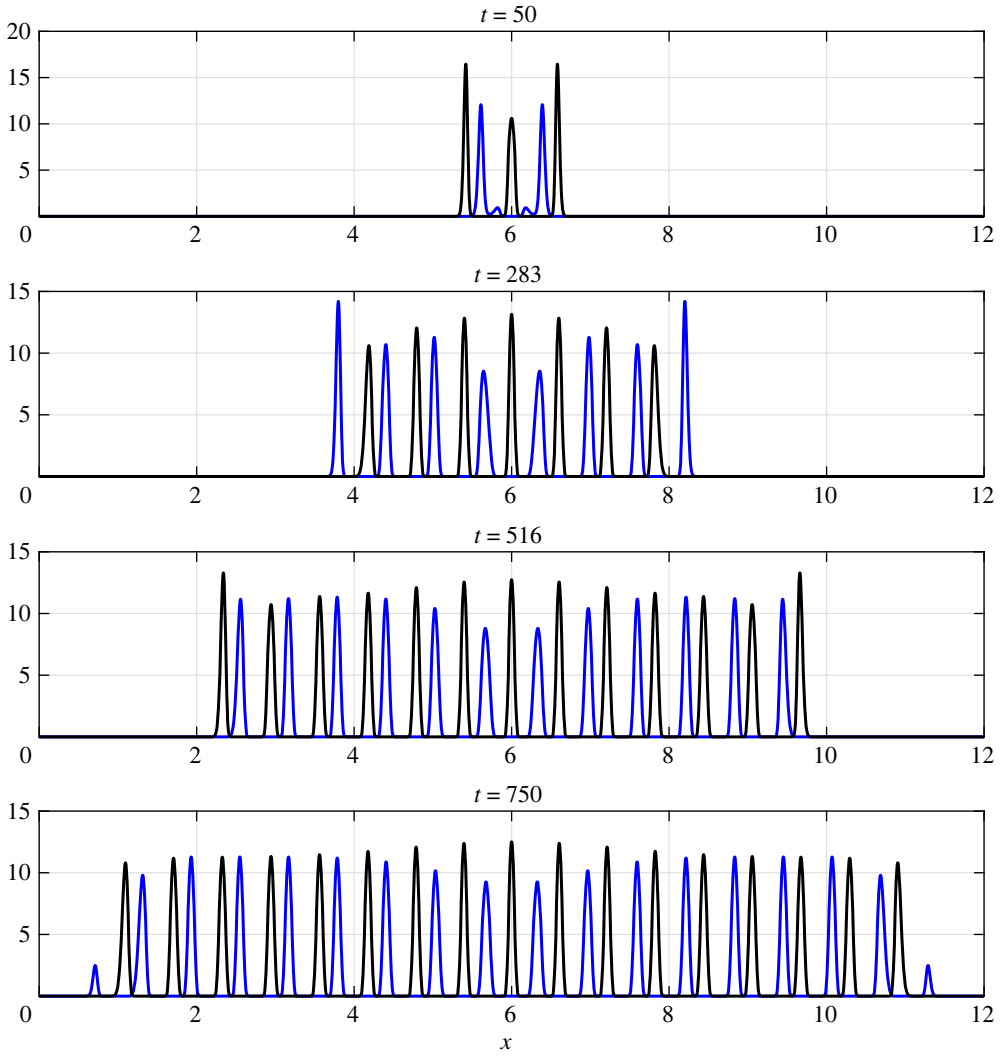

Figure 6. The numerical solution of (IVP) with $D_u = D_v = 10^{-5}$, $\alpha = 0.2$, $\beta = 0.1$ and equal initial data. The solution is shown when $t = 50, 283, 516$ and 750, with u drawn as a blue line and v a black line.

(b) Dynamics with $\alpha, \beta = O(1)$

When the coupling parameters, α and β, are much greater than $D \ll 1$, the initial development of the solution of (IVP) is more complex than that described in §2 but, as we showed in §3, once the solution develops to the point where uv is everywhere sufficiently small, the dynamics are exponentially slow. In this Section, we therefore give some examples of how the solutions segregate over an $O(1)$ time scale. We present some solutions at representative times during the evolution.[1] In each case, we have chosen $D_u = D_v = 10^{-5}$.

(i) Symmetric initial conditions

We consider localized initial conditions of the form

$$u_0(x) = v_0(x) = a\,\mathrm{e}^{-k(x-(1/2)L)^2}, \tag{4.1}$$

[1]These are best appreciated by watching the videos that can be found at electronic supplementary material (https://doi.org/10.6084/m9.figshare.c.6825659).

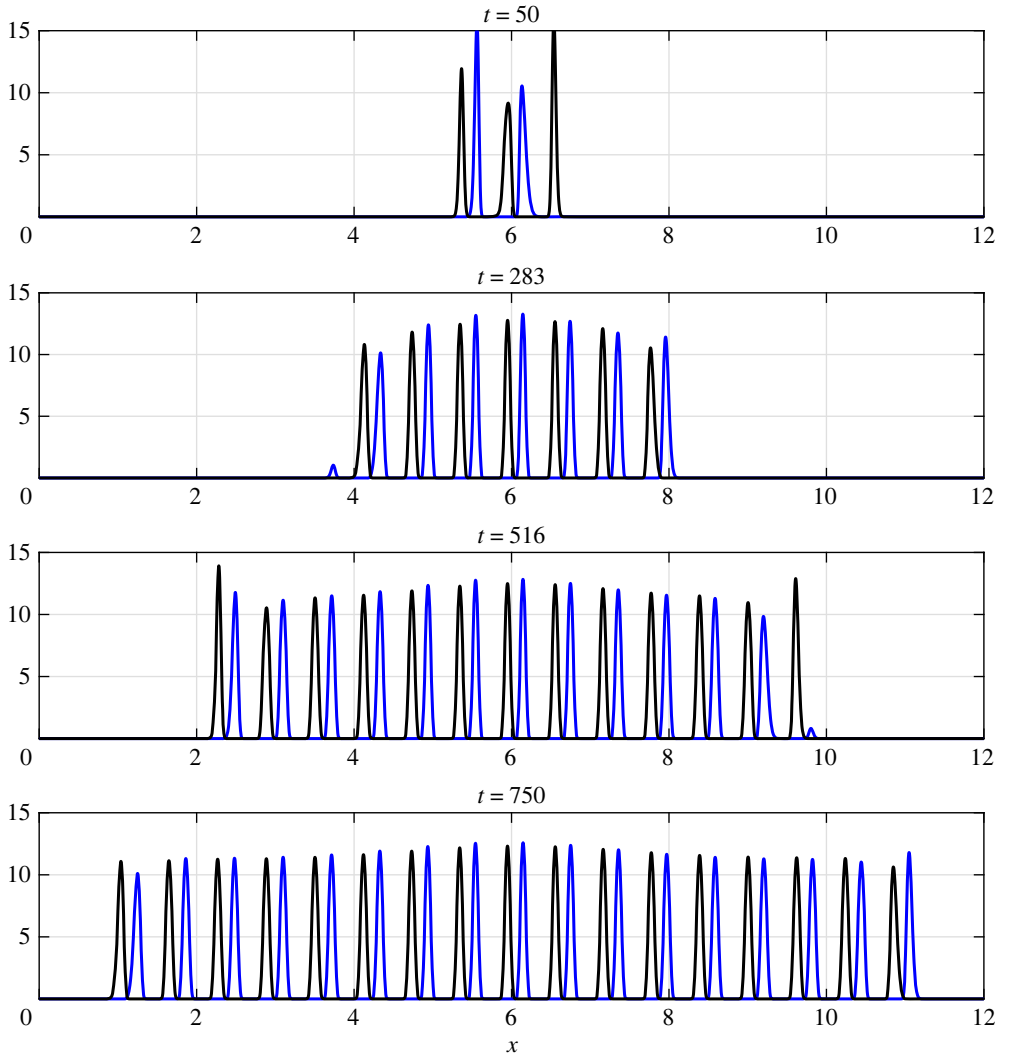

Figure 7. The numerical solution of (IVP) with $D_u = D_v = 10^{-5}$, $\alpha = 0.2$, $\beta = 0.1$ and separation parameter $x_0 = 0.025$. The solution is shown when $t = 50$, 283, 516 and 750, with u drawn as a blue line and v a black line.

with $a = 10^{-3}$ and $k = 100$. If $D_u = D_v$ and $\alpha = \beta$, (IVP) is completely symmetric, and $u(x,t) = v(x,t)$ for all $t \geq 0$. We break the symmetry by taking $\alpha \neq \beta$. Figure 5 shows the solution for $\alpha = 0.002$ and $\beta = 0.001$. Although the solution remains symmetric about the midpoint of the domain, $x = 6$, as the wavefronts spread out and leave behind them a sequence of humps, the initially overlapping humps slide apart on a time scale significantly faster than $O(D^{-1})$. Once they no longer overlap, we expect that, as predicted by the theory of §3, they continue to slide apart, but on an exponentially long time scale, which is not observable using any standard numerical solution method, so the humps appear to stick to each other in an edge touching position. In the central hump, which must remain symmetric, since $\alpha > \beta$, u is suppressed and v dominates.

Figure 6 shows the solution when α and β are each increased by a factor of 100. Now u is completely excluded in the neighbourhood of the midpoint of the domain, $x = 6$. In the region behind the wavefronts, the humps are separated and, in the solutions shown, of unequal height and spacing. Over an $O(D^{-1})$ time scale, the heights of the humps adjust to be equal and the humps themselves equally spaced, but the spacing Δ, which we have seen adjusts on

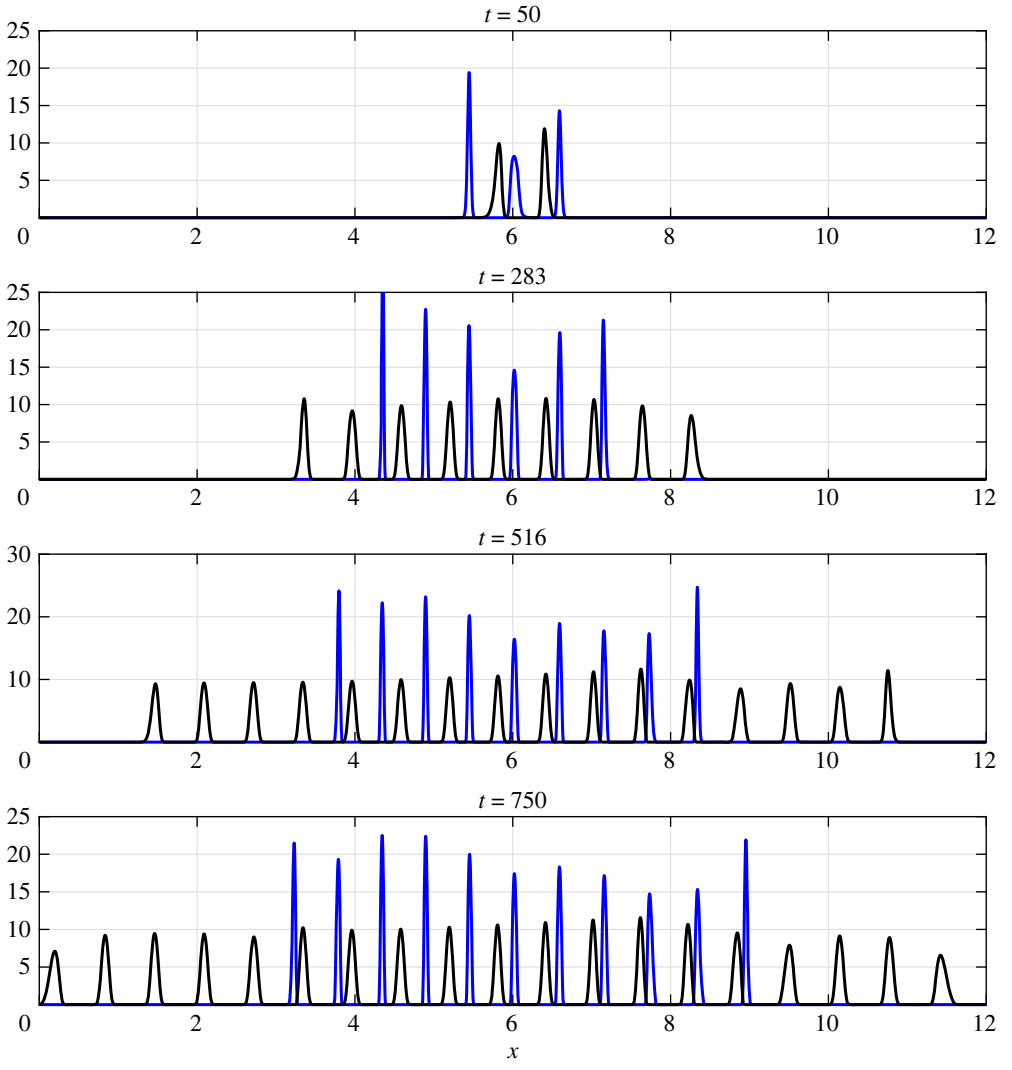

Figure 8. The numerical solution of (IVP) with $D_u = 1.25 \times 10^{-6}$, $D_v = 2 \times 10^{-5}$, $\alpha = 0.025$, $\beta = 0.2$ and separation parameter $x_0 = 0.025$. The solution is shown when $t = 50$, 283, 516 and 750, with u drawn as a blue line and v a black line.

an exponentially long time scale, remains uneven in our numerical solution for all practically realisable computation times.

(ii) Asymmetric initial conditions

Figure 7 shows the numerical solution of (IVP) with $\alpha = 0.2$ and $\beta = 0.1$, with asymmetric initial conditions

$$u_0(x) = a\,\mathrm{e}^{-k(x-(1/2)x_0-(1/2)L)^2} \quad \text{and} \quad v_0(x) = a\,\mathrm{e}^{-k(x+(1/2)x_0-(1/2)L)^2}, \tag{4.2}$$

and separation $x_0 = 0.025$. The initial interaction of u and v causes the humps to separate rapidly, and subsequent humps are formed so that they are just touching. We again predict that these will separate and become equally spaced on an exponentially long time scale.

(iii) Unequal diffusivities, $D_u \neq D_v$

Figure 8 shows the solution of (IVP) when the diffusivites of the species differ by a factor of 16. The values of α and β have been chosen to be consistent with the previous figures in this subsection. Since we have taken $D_v > D_u$, we would expect humps in v to be created faster than those in u. This is indeed what we can see in figure 8, with humps in v filling the domain of the numerical solution before the humps in u. However, we note that the final state is qualitatively similar, with a sequence of edge touching humps, and this fills the domain at a later time as the wavefronts in u continue to propagate. This is the one simulation presented here on a long domain where the periodic boundary condition does have a small effect, at least on v, but this allows us to see the slower spread of humps in u more clearly.

5. Conclusion

In this paper, we have studied the long time dynamics of the interaction of periodic structures which emerge as separated localized humps in the solution of an initial value problem for the non-local Lotka–Volterra equations with a top hat kernel and weak inter-species interactions. We have shown that, on an $O(1)$ time scale, the patterns that form are determined by the dynamics of the non-local Fisher–KPP equations that govern each individual species in isolation. We were then able to determine how the weak interaction of the two species controls the subsequent long time dynamics, which involves the separation of the humps in the solution, and is readily observable in numerical solutions until the humps are just edge-touching. The subsequent separation of the humps is exponentially slow, and not computationally accessible, but eventually leads to the symmetric disposition of the humps. For stronger interactions, the initial dynamics are coupled between the species, and lead to their mutual exclusion, but even in this case, once the humps that develop no longer overlap, the subsequent separation dynamics remain similarly exponentially slow.

There are many extensions of this system whose behaviour we will study in this series of papers, including: dynamics in two spatial dimensions; the effect of different kernel length scales; finite domain size; small, not necessarily compact, perturbations of the kernel. We are pursuing a similar programme of study of the non-local Fisher–KPP equation (see [6,8,9]).

Data accessibility. The data are provided in electronic supplementary material [10].

Declaration of AI use. We have not used AI-assisted technologies in creating this article.

Authors' contributions. D.J.N.: formal analysis, writing—original draft—review and editing; J.B.: conceptualization, software, writing—review and editing.

All authors gave final approval for publication and agreed to be held accountable for the work performed therein.

Conflict of interest declaration. We declare we have no competing interests.

Funding. No funding has been received for this article.

Appendix A. Modified theory for (IVP) with small but unequal diffusion rates

In this appendix, we modify the asymptotic theory developed in §2 to account for the situation when the diffusion rates of u and v are small but not equal. The details in region I remain unchanged, *except* that, in equations relating to functional forms for u or v, the occurrence of D is replaced by D_u or D_v respectively. In region II, firstly expansions (2.6) and (2.7) have D replaced by D_u and D_v, respectively, with $\Delta(\tau)$ and $S(\tau)$ defined as in (2.15). However, the dynamical system determining $\Delta(\tau)$ and $S(\tau)$ is modified to,

$$\Delta' = \bar{\alpha} H(\Delta, D_v) + \bar{\beta} H(\Delta, D_u) \tag{A 1}$$

and

$$S' = \frac{\bar{\alpha}\bar{\beta}}{(\bar{\alpha}+\bar{\beta})}(H(\Delta, D_v) - H(\Delta, D_u)), \tag{A 2}$$

for $\tau > 0$, with H given by (2.18). The qualitative dynamics of the modified autonomous one-dimensional dynamical system (A 1), with initial condition (2.30), determines that $\Delta(\tau)$ again has the structural dynamics detailed in §2, and we do not repeat the details here. Thereafter, $S(\tau)$ is determined by quadrature as,

$$S(\tau) = \frac{\bar{\alpha}\bar{\beta}}{(\bar{\alpha}+\bar{\beta})} \int_{\Delta_0}^{\Delta(\tau)} \frac{(H(l, D_v) - H(l, D_u))}{(\bar{\alpha}H(l, D_v) + \bar{\beta}H(l, D_u)} \, \mathrm{d}l + S_0 \quad \forall\, \tau \geq 0. \tag{A 3}$$

We observe that, on the exponentially long time scale, as $D \to 0$, we have

$$S(\tau) \to S_\infty \equiv \frac{\bar{\alpha}\bar{\beta}}{(\bar{\alpha}+\bar{\beta})} \int_{\Delta_0}^{(1/2)\lambda} \frac{(H(l, D_v) - H(l, D_u))}{(\bar{\alpha}H(l, D_v) + \bar{\beta}H(l, D_u)} \, \mathrm{d}l + S_0 \quad \text{as } \tau \to \infty. \tag{A 4}$$

References

1. Bayliss A, Volpert VA. 2015 Patterns for competing populations with species specific nonlocal coupling. *Math. Model. Nat. Phenom.* **10**, 30–47. (doi:10.1051/mmnp/201510604)
2. Segal B, Volpert V, Bayliss A. 2013 Pattern formation in a model of competing populations with nonlocal interactions. *Physica D* **253**, 12–22. (doi:10.1016/j.physd.2013.02.006)
3. Simoy MI, Kuperman MN. 2023 Non-local interaction effects in models of interacting populations. *Chaos Solitons Fract.* **167**, 112993 (doi:10.1016/j.chaos.2022.112993)
4. Tanzy M, Volpert V, Bayliss A, Nehrkorn M. 2013 Stability and pattern formation for competing populations with asymmetric nonlocal coupling. *Math. Biosci.* **246**, 14–26. (doi:10.1016/j.mbs.2013.09.002)
5. Volpert V, Udovenko O, Kuznetsov M, Banerjee M. 2022 Nonlocal reaction-diffusion equations in biomedical applications. *Acta Biotheor.* **70**, 1–28. (doi:10.1007/s10441-022-09436-4)
6. Needham DJ, Billingham J, Ladas NM, Meyer JC. 2023 The evolution problem for the 1D nonlocal Fisher-KPP equation with a top hat kernel. Part 1. The Cauchy problem on the real line. (doi:10.48550/arXiv.2304.10922)
7. Meyer JC, Needham DJ. 2014 Extended weak maximum principles for parabolic partial differential inequalities on unbounded domains. *Proc. R. Soc. A* **470**, 20140079. (doi:10.1098/rspa.2014.0079)
8. Billingham J. 2020 Slow travelling wave solutions of the nonlocal Fisher-KPP equation. *Nonlinearity* **33**, 2106–2142. (doi:10.1088/1361-6544/ab6f4f)
9. Needham DJ, Billingham J. 2023 The evolution problem for the 1D nonlocal Fisher-KPP equation with a top hat kernel. Part 2. The Cauchy problem on a finite interval. (doi:10.48550/arXiv.2304.10935)
10. Needham DJ, Billingham J. 2023 The non-local Lotka–Volterra system with a top hat kernel—Part 1: dynamics and steady states with small diffusivity. Figshare. (doi:10.6084/m9.figshare.c.6825659)